Enhancement of Red Emission ($^4F_{9/2} \rightarrow {}^4I_{15/2}$) via Upconversion in Bulk and Nanocrystalline Cubic $Y_2O_3:Er^{3+}$

John A. Capobianco,* Fiorenzo Vetrone, and J. Christopher Boyer

Department of Chemistry and Biochemistry, Concordia University, 1455 de Maisonneuve Blvd. W, Montreal, Canada

Adolfo Speghini and Marco Bettinelli

Dipartimento Scientifico e Tecnologico, Università di Verona, Ca' Vignal, Strada Le Grazie 15, I-37134 Verona, Italy

Received: August 1, 2001; In Final Form: October 23, 2001

In this paper, we investigate as a function of erbium concentration (1, 2, 5, 10 mol %) the upconversion properties of bulk and nanocrystalline Er^{3+} doped cubic Y_2O_3. After excitation at short wavelength (488 nm) or with upconversion pumping (815 nm), green and red emissions were observed for both nanocrystalline and bulk samples in the visible region of the spectrum, while blue emission was observed in bulk $Y_2O_3:Er^{3+}$ only. The upconverted emission after 815 nm excitation revealed an enhancement of the red [$^4F_{9/2} \rightarrow {}^4I_{15/2}$] emission with respect to the green [($^2H_{11/2}$, $^4S_{3/2}$) $\rightarrow {}^4I_{15/2}$] emission when the dopant concentration is increased. However, the magnitude of the red enhancement in the bulk material differs slightly from its nanocrystalline counterpart, with the nanocrystalline material showing a higher degree of dependence on the dopant Er^{3+} concentration. It is believed that two distinct mechanisms are responsible for populating the $^4S_{3/2}$ and $^4F_{9/2}$ levels, with the latter being more efficient at higher Er^{3+} ion concentration.

Introduction

It has been widely demonstrated that the reduction of particle size of crystalline systems leads to important modifications of some of their bulk properties.[1,2] Nanocrystalline materials with particle diameters of 100 nm or less can exhibit novel physical properties, in particular an increased luminescence efficiency, that are not observed in their bulk counterparts.[3] Taking advantage of these size-induced changes, the design of enhanced materials for advanced phosphor and photonic applications becomes possible.[4] It is conceivable that these materials may find a wide range of uses in light-emitting diodes, photovoltaics, and lasers.

Lanthanide-doped yttria (Y_2O_3) are common phosphors in optical display and lighting applications, and the search for new phosphors has led to the preparation of nanocrystalline forms of Y_2O_3.[5] Over the past decade, much attention has been given to two well-known phosphors, $Y_2O_3:Eu^{3+}$ [2,4−6] and $Y_2O_3:Tb^{3+}$.[3,7−9] Bhargava et al. have observed an increase in the photoluminescent efficiency of the characteristic green $^5D_4 \rightarrow {}^7F_5$ emission of Tb^{3+}-doped yttrium oxide nanocrystals as the size of the crystals decreases.[3,10] Following this, Tissue et al. have done a considerable amount of work on nanophase monoclinic $Y_2O_3:Eu^{3+}$, showing that the lifetime of the $^5D_0 \rightarrow {}^7F_1$ lifetime is particle-size-dependent.[11]

The current interest in upconversion materials and, as a result, in upconversion processes is fueled by the potential of these systems as phosphor or laser materials. In recent years, advances in both solid-state lasers and semiconductor laser diodes have resulted in more efficient IR sources. As a result, upconversion, where the absorption of two or more low energy photons is followed by the emission of a higher energy photon, has garnered significant attention. Due to the availability of low-cost near-infrared (NIR) laser diodes, conversion of infrared radiation to visible has generated much of the current interest in upconversion. Tripositive erbium is an excellent candidate for upconversion since the $4f^n$ electronic levels provide intermediate levels, which are easily accessible with NIR radiation.[12] For example, there are two levels in the NIR ($^4I_{9/2}$ and $^4I_{11/2}$) around 800 and 980 nm, which can be conveniently populated by such diodes. There exist various processes, which can lead to emission at wavelengths shorter than the excitation wavelength. In general, the most efficient are energy-transfer upconversion (ETU) and excited-state absorption (ESA) processes in the case of the Er^{3+} ion.

In this paper, we report a very efficient infrared-to-visible upconversion in nanocrystalline and bulk cubic $Y_2O_3:Er^{3+}$. The Er^{3+} doped Y_2O_3 nanocrystals may have application for two-photon imaging in confocal microscopy and crystals of the bulk material in single wavelength pumped upconversion laser.[13]

Experimental Section

Nanosized cubic Y_2O_3 crystals doped with 1, 2, 5, and 10 mol % Er_2O_3 ($Y_{1.98}Er_{0.02}O_3$, $Y_{1.96}Er_{0.04}O_3$, $Y_{1.90}Er_{0.10}O_3$, and $Y_{1.80}Er_{0.20}O_3$, respectively) were prepared using a solution combustion (propellant) synthesis procedure.[14,15] Details of the synthesis have been given in a previous article.[16] The synthesis reaction is

$$6M(NO_3)_3 + 10NH_2CH_2COOH + 18O_2 \rightarrow 3M_2O_3 + 5N_2 + 18NO_2 + 20CO_2 + 25H_2O$$

* Correspondening author. Telephone: +1-514-848-4327. Fax: +1-514-848-2868. E-mail: capo@vax2.concordia.ca.

10.1021/jp0129582 CCC: $22.00
Published on Web 01/18/2002

where M = Y, Er. A glycine-to-metal nitrate molar ratio of 1.2:1 was employed to prepare the aqueous precursor solution.

For purposes of comparison, bulk samples doped with 1, 2, 5, and 10 mol % Er_2O_3 ($Y_{1.98}Er_{0.02}O_3$, $Y_{1.96}Er_{0.04}O_3$, $Y_{1.90}Er_{0.10}O_3$, and $Y_{1.80}Er_{0.20}O_3$, respectively) were prepared by intimately mixing Y_2O_3 (Aldrich, 99.99%) and Er_2O_3 (Aldrich, 99.99+ %), pressing the powders into pellets under 10 tons of pressure and firing them in air at 1500 °C for 48 h. At this temperature, the optimum homogeneity (verified using scanning electron microscopy) was obtained.

All yttria samples were kept in air without any further precaution.

In a recent paper, using X-ray diffraction (XRD), it was shown that the propellant synthesis of $Y_{1.80}Nd_{0.20}O_3$ and $Y_{1.80}Er_{0.20}O_3$, carried out in the same conditions used in the present study, yields cubic nanocrystals with an average size of 5−20 nm.[15] These results have been confirmed by small-angle X-ray scattering (SAXS) and transmission electron microscopy (TEM) measurements on the same materials,[17] which have also shown that they form polycrystalline aggregates with mass fractal properties. A further detailed investigation using wide-angle X-ray scattering (WAXS) and TEM[18] has shown that the average size of the Y_2O_3 crystallites obtained by the procedure described above is not influenced strongly by either the nature or concentration of the Ln^{3+} dopant. Therefore, in the discussion herein, we can safely assume that the average radius of the crystallites of all the nanostructured samples is in the range 5−20 nm, whereas the size of the particles in the bulk sample is at least 10 times larger.

The diffuse reflectance spectrum in the medium infrared (MIR) region was measured at room temperature with a Nicolet Magna 760 FTIR spectrometer using an aluminated mirror as a reference.

Luminescence spectra were measured by exciting either at 488 nm using a Coherent Sabre Innova, 20 W argon ion laser, or at 815 nm using a Spectra-Physics Model 3900 Titanium Sapphire pumped by the 514 nm line of a Coherent Sabre Innova argon ion laser. The visible emissions were then collected and dispersed using a Jarrel-Ash 1-meter Czerny Turner double monochromator. The signals were monitored with a thermoelectrically cooled Hamamatsu R43-02 photomultiplier tube. The photomultiplier signals were processed by a preamplifier model SR440 Stanford Research System.[5] A gated photon counter model SR400 Stanford Research Systems data acquisition system was used as an interface between the computer and the spectroscopic hardware. The signal was recorded under computer control using the Stanford SR465 software data acquisition/analyzer system.

Results and Discussion

In a previous paper,[16] we have shown the reflectance, emission, and upconversion spectra for the 10 mol % bulk and nanocrystalline cubic Y_2O_3:Er^{3+} samples. In the present paper, we extend the spectroscopic investigation by studying the effects of Er^{3+} concentration (1, 2, 5, and 10 mol %) on the upconversion emission properties of bulk and nanocrystalline cubic Y_2O_3.

Stokes Luminescence Spectroscopy (λ_{exc} = 488 nm). The visible luminescence spectra of bulk and nanocrystalline $Y_{2-x}Er_xO_3$ are shown in Figures 1 and 2, respectively. Bands are observed in the 550 and 675 nm region of the spectra and are assigned to the transitions from the thermalized ($^2H_{11/2}$, $^4S_{3/2}$) and $^4F_{9/2}$ excited states, respectively, to the $^4I_{15/2}$ ground state of Er^{3+} ions in the C_2 and C_{3i} sites. This is in good agreement

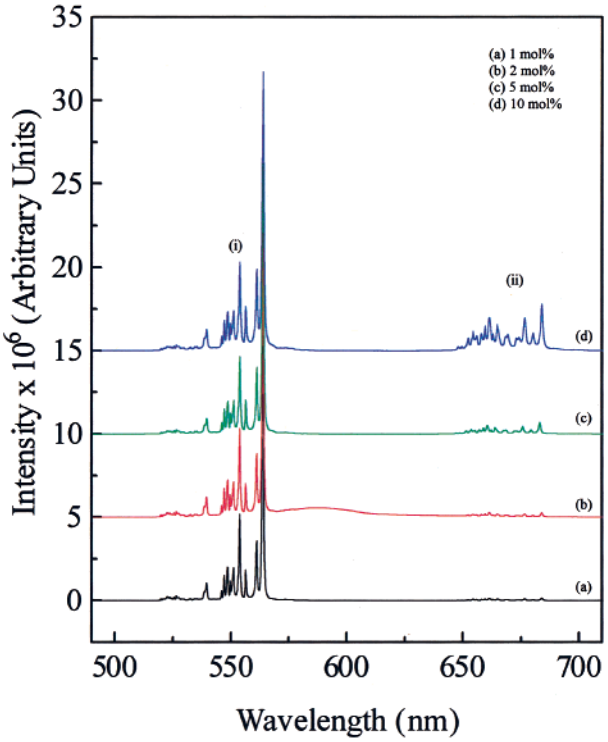

Figure 1. Room-temperature luminescence of bulk Y_2O_3:Er^{3+} upon excitation at 488 nm. (i) ($^2H_{11/2}$, $^4S_{3/2}$) → $^4I_{15/2}$ and (ii) $^4F_{9/2}$ → $^4I_{15/2}$.

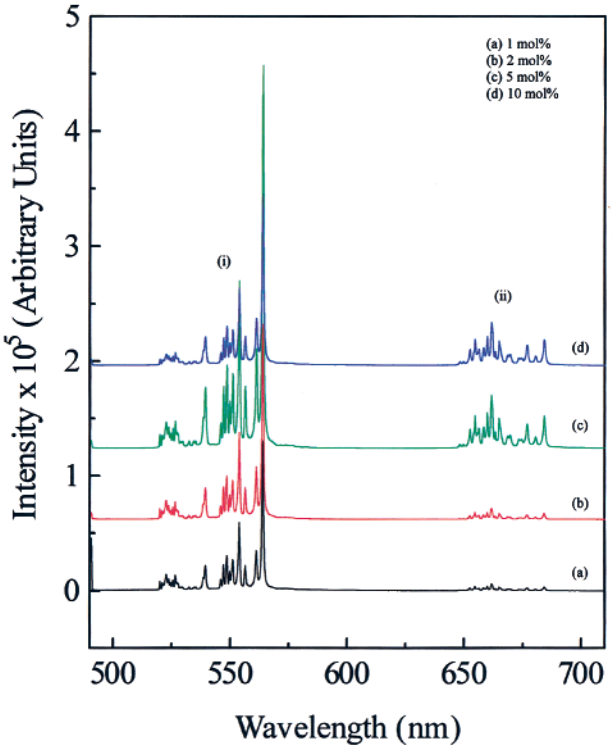

Figure 2. Room-temperature luminescence of nanocrystalline Y_2O_3:Er^{3+} upon excitation at 488 nm. (i) ($^2H_{11/2}$, $^4S_{3/2}$) → $^4I_{15/2}$ and (ii) $^4F_{9/2}$ → $^4I_{15/2}$.

with previous experimental[19] and theoretical[20] studies. Cubic Y_2O_3 crystallizes in the *C* bixbyite structure, with space group *Ia*3 (T_h^7).[21,22] It has been shown that the Y^{3+} ions are accommodated in 32 sites in the unit cell; 24 sites with point group symmetry C_2 and 8 sites with C_{3i} symmetry. In general, Ln^{3+} ions have been found to be distributed randomly in both sites in Y_2O_3 single crystals.[23] However, in a recent paper,[24]

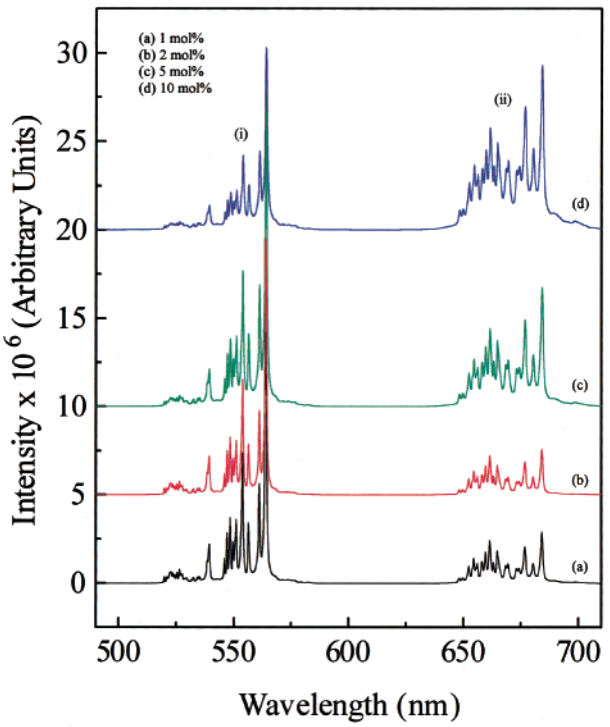

Figure 3. Upconverted emission of bulk Er^{3+} doped Y_2O_3 at room temperature, showing (i) ($^2H_{11/2}$, $^4S_{3/2}$) → $^4I_{15/2}$ and (ii) $^4F_{9/2}$ → $^4I_{15/2}$, λ_{exc} = 815 nm.

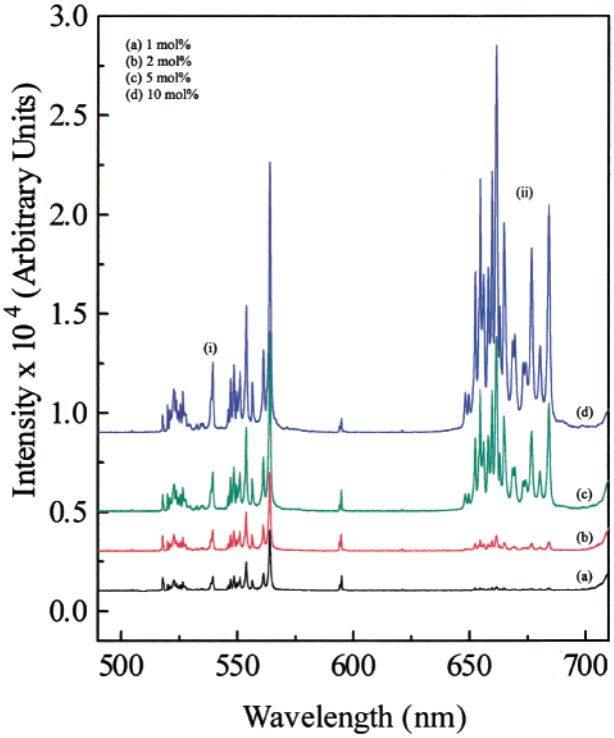

Figure 4. Upconverted emission of Er^{3+} doped Y_2O_3 nanocrystals at room temperature, showing (i) ($^2H_{11/2}$, $^4S_{3/2}$) → $^4I_{15/2}$ and (ii) $^4F_{9/2}$ → $^4I_{15/2}$, λ_{exc} = 815 nm.

^{151}Eu Mossbauer studies on nanocrystalline $Y_2O_3:Eu^{3+}$ and $Gd_2O_3:Eu^{3+}$, prepared by propellant synthesis, revealed that there is a preferential occupation of the dopant ions in the C_{3i} site. This site has associated with it a center of inversion; therefore, according to the selection rules, f−f electric dipole transitions are forbidden. Consequently, the major contribution to the intensity of the observed transitions originates from Er^{3+} ions in the C_2 sites.

Anti-Stokes (Upconversion) Luminescence Spectroscopy Following Excitation into the $^4I_{9/2}$ level (λ_{exc} = 815 nm). Continuous wave excitation with NIR radiation (815 nm) into the $^4I_{9/2}$ ← $^4I_{15/2}$ transition of the bulk and nanocrystalline samples produced intense luminescence peaks in the visible region (Figures 3 and 4). The peaks were assigned to the following transitions: green emission in the 520−570 nm region assigned to the ($^2H_{11/2}$, $^4S_{3/2}$) → $^4I_{15/2}$ transition and red emission in the 650−700 nm region assigned to the $^4F_{9/2}$ → $^4I_{15/2}$ transition for Er^{3+} ions in the C_2 and C_{3i} sites of Y_2O_3. Also, it should be noted that a relatively weak blue emission was observed in bulk $Y_2O_3:Er^{3+}$ (Figure 5). The peaks were assigned to the $^4F_{5/2}$ → $^4I_{15/2}$ and $^4F_{7/2}$ → $^4I_{15/2}$ transitions in the 450−465 and 485−505 nm regions, respectively. We have also observed a manifold in the 468−480 nm region and have assigned it to the intraconfigurational $^2P_{3/2}$ → $^4I_{11/2}$ transition. No blue emission was observed in the nanocrystalline samples.

After irradiating the nanocrystalline material with 815 nm, we notice primarily that the absolute intensities of the ($^2H_{11/2}$, $^4S_{3/2}$) → $^4I_{15/2}$ and $^4F_{9/2}$ → $^4I_{15/2}$ transitions are very weak in the 1 mol % sample when compared to the sample with 10 mol % dopant concentration. However, as the Er^{3+} dopant concentration is increased, the upconversion luminescence becomes more intense. At this point, we should note that the bulk samples do not follow the same general trend as their nanocrystalline counterparts. In the bulk material, the absolute intensities of the ($^2H_{11/2}$, $^4S_{3/2}$) → $^4I_{15/2}$ and $^4F_{9/2}$ → $^4I_{15/2}$ transitions increase up to 5 mol % and then decrease in absolute intensity for the 10 mol % sample (Figure 3).

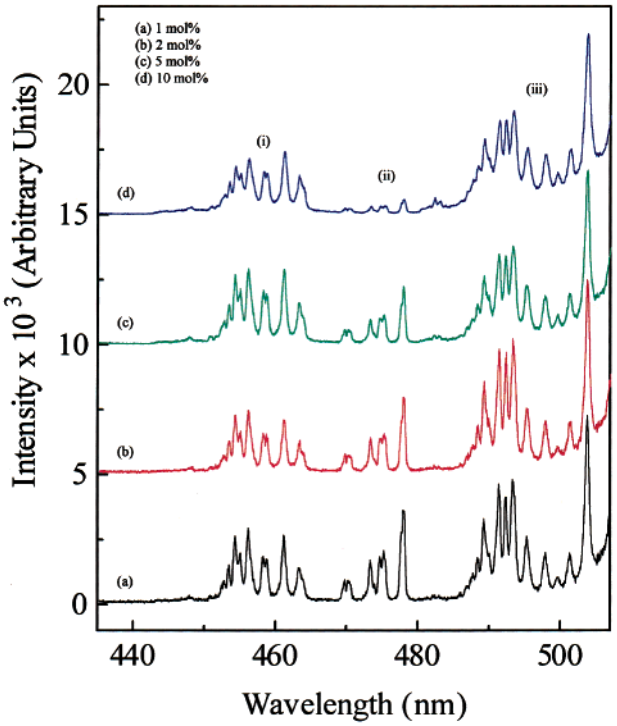

Figure 5. Upconverted emission of bulk $Y_2O_3:Er^{3+}$ at room temperature, showing (i) $^4F_{5/2}$ → $^4I_{15/2}$, (ii) $^2P_{3/2}$ → $^4I_{11/2}$, and (iii) $^4F_{7/2}$ → $^4I_{15/2}$ (λ_{exc} = 815 nm).

Furthermore, we have observed an enhancement of red emission upon 815 nm excitation. The intensity of the red ($^4F_{9/2}$ → $^4I_{15/2}$) emission increases at a more rapid rate than that of the green [($^2H_{11/2}$, $^4S_{3/2}$) → $^4I_{15/2}$] emission. In fact, the

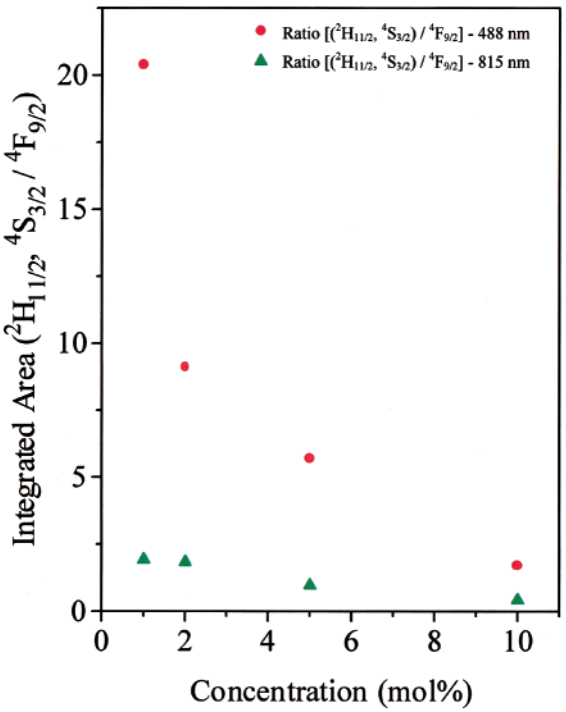

Figure 6. Graph of the ratio of the integrated areas of the ($^2H_{11/2}$, $^4S_{3/2}$) $\rightarrow$ $^4I_{15/2}$ and $^4F_{9/2} \rightarrow {}^4I_{15/2}$ bands [($^2H_{11/2}$, $^4S_{3/2}$)/$^4F_{9/2}$] vs Er^{3+} concentration for the bulk material.

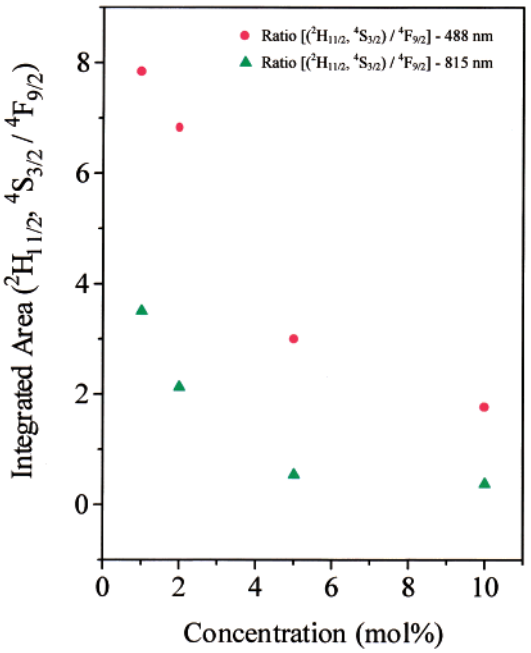

Figure 7. Graph of the ratio of the integrated areas of the ($^2H_{11/2}$, $^4S_{3/2}$) $\rightarrow$ $^4I_{15/2}$ and $^4F_{9/2} \rightarrow {}^4I_{15/2}$ bands [($^2H_{11/2}$, $^4S_{3/2}$)/$^4F_{9/2}$] vs Er^{3+} concentration for the nanocrystalline material.

enhancement of the red emission is clearly evident upon comparing the calculated relative intensities of the ($^2H_{11/2}$, $^4S_{3/2} \rightarrow {}^4I_{15/2}$) and ($^4F_{9/2} \rightarrow {}^4I_{15/2}$) transitions. In the nanocrystalline material, the 1 mol % sample has a relative (Green:Red) intensity ratio of 3.5:1. As the dopant concentration is increased, the red component becomes more prominent which affects the relative intensity ratio. For example, in the 10 mol % sample, the ratio becomes 1:2.7. In the bulk material, the enhancement is slightly less prominent. In the 1 mol % sample, we obtain a ratio of 3:1, while in the 10 mol % sample, the ratio is approximately 1:1. From this observation, we postulate that the channel populating the red upconversion is more concentration-dependent in the nanocrystalline material, prepared by propellant synthesis, than that for its bulk counterpart.

While the relative enhancement of the red emission ($^4F_{9/2} \rightarrow {}^4I_{15/2}$) is observed in the upconverted luminescence, it was also observed in the Stokes luminescence spectra. However, the effect of the $^4F_{9/2}$ enhancement is clearly much more pronounced when exciting at 815 nm. This is demonstrated in Figures 6 and 7, which show a graph of the ratio of the integrated intensity of the green emission [($^2H_{11/2}$, $^4S_{3/2}$) $\rightarrow {}^4I_{15/2}$] over that of the red emission [$^4F_{9/2} \rightarrow {}^4I_{15/2}$], versus Er^{3+} concentration, for the bulk and nanocrystalline samples at both (488 and 815 nm) wavelengths. We observe that for both the bulk and nanocrystalline samples, as the dopant concentration is increased, the difference in ratios becomes less significant.

Comparison of the Stokes (λ_{exc} = 488 nm) and Upconversion (λ_{exc} = 815 nm) Spectra. Comparison of the peak shapes in both the upconversion and Stokes spectra for all bulk samples under investigation shows no dissimilarities. The same is also observed for the nanocrystalline samples. That is, the peak shape is insensitive to dopant concentration or pump wavelength. While the overall peak shape is the same, the relative intensities of several peaks are significantly different. In particular, we notice that the peaks at $\lambda = 670$ nm are clearly more intense for the bulk material. This difference in the relative intensities within the manifolds may be attributed to the vibronic transitions associated with the C_{3i} sites, which may be stronger in the bulk sample due to more favorable electron−phonon coupling.[16]

Although the spectra are identical and unaffected by the pump wavelength, 488 or 815 nm, there is a notable reduction in the overall luminescence when pumping with 815 nm. We have shown in a previous paper[16] that yttria nanoparticles prepared by the above-mentioned combustion (propellant) synthesis adsorb CO_2 and H_2O. In fact, both CO_2 and H_2O are products of the combustion reaction and could therefore be adsorbed immediately after the formation of the nanoparticles. The MIR spectrum of the yttria nanoparticles shows bands at approximately 1500 and 3350 cm^{-1} due to vibrational modes typical of carbonates and hydroxyl ions, respectively. The presence of these groups on the surface yields vibrational quanta of relatively high wavenumbers compared to the phonons of pure yttria (phonon cutoff $\approx$ 600 cm^{-1}), which are the only ones available in the bulk. The rate of multiphonon relaxation is dependent upon the energy gap separating the upper and lower states and the highest phonon energy in the material.[25] The rate of the multiphonon relaxation can be expressed as[26]

$$W_{MPR} = C \exp(-\alpha \Delta E) \qquad (1)$$

where ΔE is the energy gap to the next lower level and the parameters C and α are constants and can be derived from the measurements of the luminescence decay times and the calculation of the radiative transition rates. It follows that in the nanocrystalline material, the presence of vibrational quanta of about 1500 and 3350 cm^{-1} makes multiphonon relaxation much more probable than that in the bulk material. Therefore, in the nanocrystalline material, the ions relax through the emission of phonons rather than the emission of photons. For example, the energy gap separating $^4S_{3/2}$ from the lower lying $^4F_{9/2}$ manifold is approximately 2800 cm^{-1}. In the nanocrystalline material, the presence of vibrational quanta of about 1500 and 3350 cm^{-1} makes multiphonon relaxation of ($^2H_{11/2}$, $^4S_{3/2}$) much more

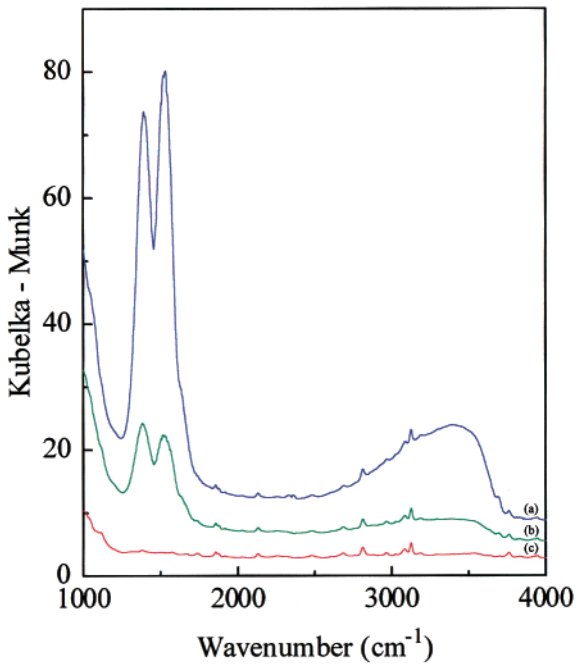

Figure 8. Diffuse reflectance spectra of nanocrystalline $Y_{1.8}Er_{0.2}O_3$ following sequential heat treatment: (a) 800 °C for 17 h, (b) 1000 °C for 65 h, and (c) bulk $Y_{1.8}Er_{0.2}O_3$ sample shown for comparison.

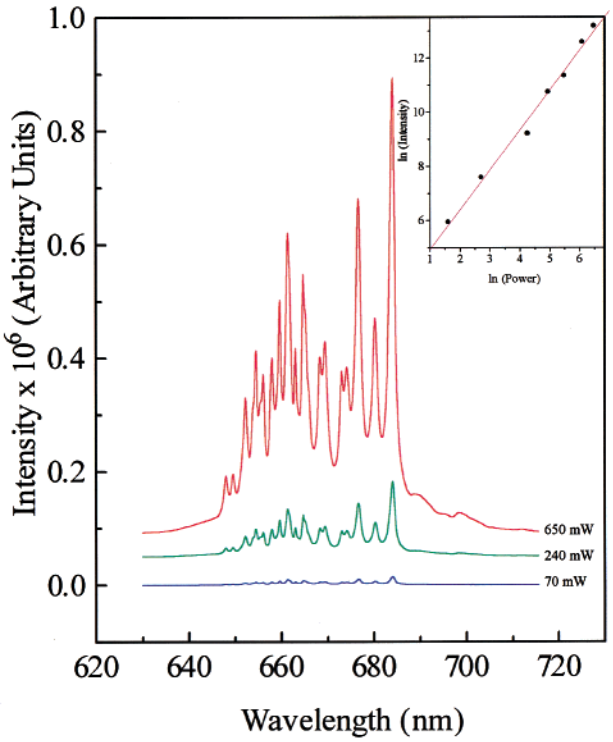

Figure 9. Power study of the $^4F_{9/2} \rightarrow {}^4I_{15/2}$ transition in 10 mol % bulk $Y_2O_3:Er^{3+}$ (λ_{exc} = 815 nm). Inset: Power dependence of the upconversion luminescence intensity observed with 815 nm excitation.

probable than that for the bulk sample, where at least four phonons are required to bridge the same gap.

To reduce the amount of CO_3^{2-} and OH^- ions on the surface of the nanoparticles, different heat treatments on a nanocrystalline $Y_{1.8}Er_{0.2}O_3$ sample were carried out. First, the sample was treated at 800 °C for 17 h and then cooled to room temperature. Then, the same sample was treated at 1000 °C for 65 h and then cooled to room temperature. Figure 8 shows the MIR spectra of the doped nanoparticles after the first and the second heat treatment as well as a bulk sample for comparison. Both the spectra of nanocrystalline yttria samples show bands at approximately 1500 and 3350 cm^{-1}, which indicate the presence of adsorbed CO_2 and H_2O, respectively. On the other hand, the bulk sample shows no bands at 1500 and 3350 cm^{-},[1] indicating the lack of adsorption of CO_2 and H_2O. After the second heat treatment, the overall intensities of the bands at 1500 and 3350 cm^{-1} indicate that the heat treatments did reduce the overall surface contamination, but in the present experimental conditions, the contaminants were not completely removed. On the other hand, a longer heat treatment at higher temperatures could induce an aggregation of the nanoparticles, a process in which they combine to form larger particles. In this case, as the spectroscopy of the nanocrystalline material is particle-size-dependent, a comparison between the luminescence of the heat-treated and nonheat treated nanocrystalline materials could be difficult to make.

Red and Green Upconversion. As we have shown in Figures 3 and 4, the upconverted luminescence intensity increases as a function of the Er^{3+} concentration. It is quite clear that the upconversion process is concentration-dependent. The mechanism can take place through either an energy transfer (ET) process or via excited state absorption (ESA) since, it is well-known that both processes are dependent upon dopant concentration. The concentration dependence can be readily discerned as in the more dilute samples, the $Er^{3+}-Er^{3+}$ distances are far to large for any effective ion−ion interactions to take place.

Since there are more Er^{3+} ions available at higher concentrations, one may postulate substantial energy transfer can thus occur, since the energy transfer rate is strongly dependent on the distance between the ions involved. However, since upconversion does occur in the dilute samples, we must assume that both energy transfer upconversion (ET) and the excited-state absorption (ESA) occur concomitantly.

To obtain a better understanding of the mechanism(s) of upconversion, a power dependence study of the luminescence intensity versus pump power was performed (Figure 9). It has been shown[27] that the intensity of the upconverted luminescence, I_o, is proportional to some power n of the excitation intensity I_i, i.e., $I_o \propto I_i^n$, where $n = 2, 3...$ For the interpretation of the upconverted luminescence, it is often assumed that n is the order of the upconversion process. More specifically, n is, under normal circumstances,[28] the number of pump photons required to populate the emitting state and is determined from the slope of the line of the graph, ln intensity versus ln pump power. The fitting of the data yields a straight line with a slope of approximately 2 for the $(^2H_{11/2}, {}^4S_{3/2}) \rightarrow {}^4I_{15/2}$ and $^4F_{9/2} \rightarrow {}^4I_{15/2}$ transitions in all the samples under investigation. It was therefore determined that the upconversion occurs via a two-photon process. No inflection was observed in the power study, and therefore, photon avalanche was ruled out as a possible mechanism for upconversion.[29]

The population of the higher energy levels after NIR pumping is relatively well-known and usually occurs by two independent processes, ET and ESA. The mechanism for red and green upconversion is as follows: The laser light brings the Er^{3+} ion to the $^4I_{9/2}$ level, which then nonradiatively decays into the $^4I_{11/2}$ level. After this nonradiative relaxation, either an energy transfer from a neighboring Er^{3+} ion in the $^4I_{9/2}$ state or a second photon from the incident laser beam brings the ion to the $^4F_{3/2}$ level.[30,31] Alternatively, after the initial excitation, the Er^{3+} ion can nonradiatively decay down to the $^4I_{13/2}$ level. Again, either an energy transfer process from another Er^{3+} ion in the $^4I_{9/2}$ state or a second photon populates the $^2H_{11/2}$ level. Emission from

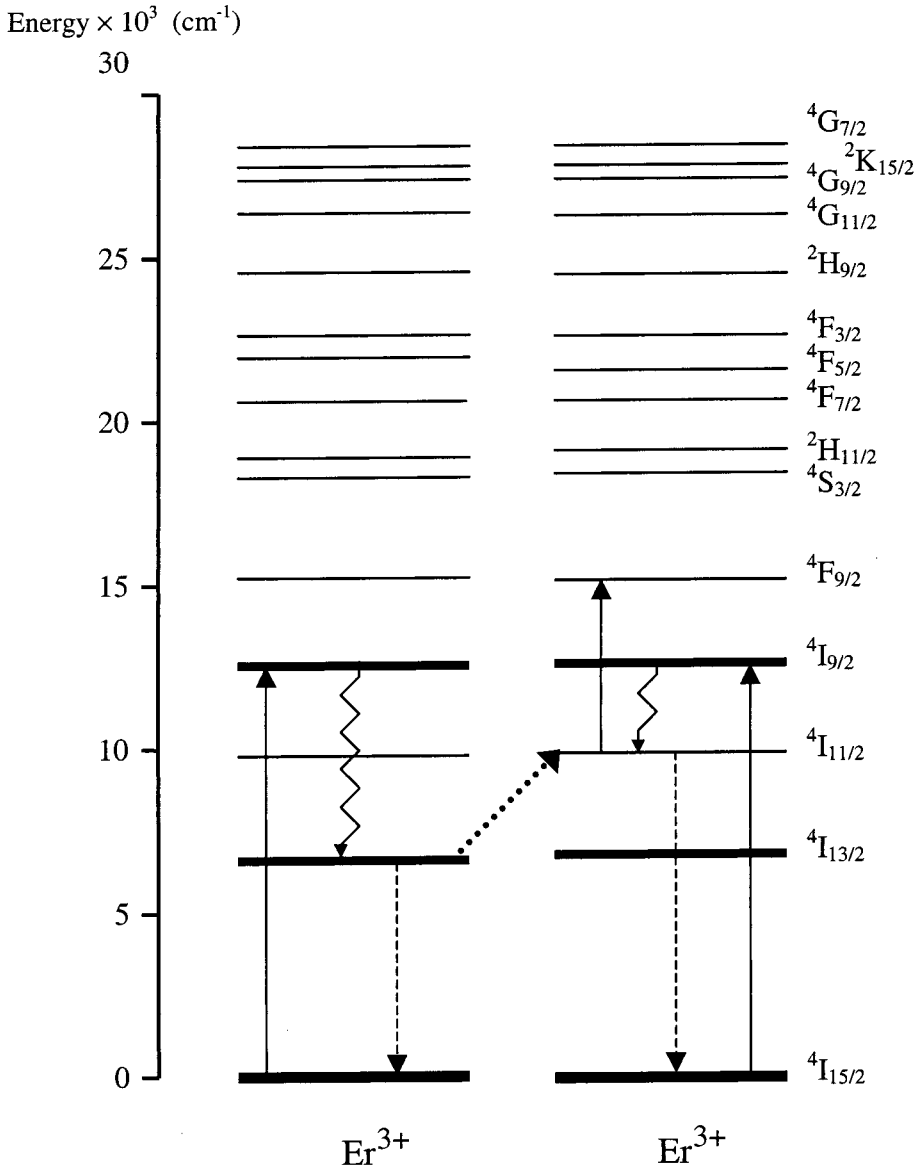

Figure 10. Energy level diagram of Er^{3+} ions in Y_2O_3 showing the two photon energy transfer upconversion process responsible for populating the $^4F_{9/2}$ level ($\lambda_{exc} = 815$ nm).

the lower lying states can then observed. We should note here that there is not perfect resonance between the initial and final states in the energy transfer mechanism. As a result, the emission or absorption of one or more phonons compensates for this mismatch in energy. Thus, we can state that the energy transfer mechanism responsible for populating the ($^2H_{11/2}$, $^4S_{3/2}$) $\rightarrow$ $^4I_{15/2}$, and $^4F_{9/2} \rightarrow {}^4I_{15/2}$ transitions is a phonon-assisted energy transfer process (PET).

If upconversion occurs only via the above mechanisms, we would then expect upconversion spectra with identical relative intensities as in the Stokes luminescence spectra ($\lambda_{exc} = 488$ nm). This is clearly not the case, as we observe an enhancement of the red emission for the $^4F_{9/2}$ state with increasing Er^{3+} concentration. Chen et al.[31] have also observed an enhancement of the red emission for the upconversion of Er^{3+} in Gadolinium Gallium Garnet (GGG). It was postulated that a second mechanism is responsible for populating the $^4F_{9/2}$ level only (Figure 10). The laser light (815 nm) excites the $^4I_{9/2}$ state and nonradiative relaxation occurs to the $^4I_{11/2}$ state. Phonon-assisted energy transfer occurs via two transitions: $^4I_{9/2} \rightarrow {}^4I_{13/2}$ and $^4I_{11/2} \rightarrow {}^4F_{9/2}$, resulting in the population of the $^4F_{9/2}$ state. This behavior can occur because these two mechanisms could be of different multipolar nature and therefore do not depend in the same way on the dopant concentration. As a result, the latter mechanism would be more effective as the Er^{3+} concentration is increased.[31]

Blue Upconversion. In bulk and nanocrystalline cubic Y_2O_3:Er^{3+}, we have shown that the mechanism resulting in green ($^2H_{11/2}$, $^4S_{3/2}$) and red ($^4F_{9/2}$) upconversion occurs via two distinct processes acting simultaneously; a phonon-assisted energy transfer (PET) process and an excited state absorption (ESA) process. However, we cannot readily exclude the possibility of even more upconversion mechanisms occurring to populate the higher energy levels. We observe emission from the $^2P_{3/2}$ level, which is much higher in energy than either the $^4F_{3/2}$ or $^2H_{11/2}$ states that are populated by the mechanisms previously described. Therefore, it follows from this that another mechanism must be operative to populate the high-energy $^2P_{3/2}$ level. This hypothesis was elucidated by the power study of the blue intraconfigurational $^2P_{3/2} \rightarrow {}^4I_{11/2}$ transition. While the power dependence study of the $^4F_{5/2,\ 7/2} \rightarrow {}^4I_{11/2}$ transitions revealed a quadratic dependence on the pump power, the power study of

the $^2P_{3/2} \rightarrow {}^4I_{11/2}$ transition revealed a cubic dependence. That is, a three-photon mechanism is responsible for populating the $^2P_{3/2}$ upper state.

The $^2P_{3/2}$ state is populated via another ESA process and occurs by the following mechanism. First, the 815 nm light excites the Er^{3+} ion to the $^4I_{9/2}$ multiplet, after which the Er^{3+} ion relaxes to the $^4I_{11/2}$ level by a nonradiative process. A second and third photon excites the Er^{3+} ion to the $^4G_{7/2}$ level. Again, nonradiative decay results in the population of the $^2P_{3/2}$ level and of course the ($^2H_{11/2}$, $^4S_{3/2}$) and $^4F_{9/2}$ levels.

From the upconversion spectra, it was revealed that PET and ESA are simultaneously occurring to populate the red and green upper states. From the upconversion spectra of the bulk material in the blue region, we observed that the relative intensity of the $^2P_{3/2} \rightarrow {}^4I_{11/2}$ and the $^4F_{5/2,\ 7/2} \rightarrow {}^4I_{15/2}$ transitions is approximately 1:1:1 in the 1 mol % sample. However, as the concentration of Er^{3+} dopant is increased, the intensities of the $^4F_{5/2} \rightarrow {}^4I_{15/2}$ and $^4F_{7/2} \rightarrow {}^4I_{15/2}$ transitions increase, while the intensity of the $^2P_{3/2} \rightarrow {}^4I_{11/2}$ remains unchanged. We believe that the $^4F_{5/2}$ and $^4F_{7/2}$ levels are populated by nonradiative relaxation from the $^4F_{3/2}$ state via the two photon PET process described earlier, while the $^2P_{3/2}$ level is populated by a three-photon ESA process. As a result of this hypothesis, we postulate that at low Er^{3+}concentrations, the dominant mechanism is ESA process populating the $^2P_{3/2}$ level, as the Er^{3+} ions are too far apart for any substantial energy transfer to take place. However, as the concentration of the dopant is increased, there are more Er^{3+} ions available and in closer proximity. Thus, substantial energy transfer can then take place. So we believe that at high dopant concentrations, the PET process "takes over" and becomes the dominant upconversion mechanism.

Conclusions

In this paper, we have reported on the detailed investigation of the near-infrared excited upconversion emission as well as the mechanisms responsible for pumping the upper levels in bulk and nanocrystalline cubic $Y_2O_3:Er^{3+}$. We have shown that an enhancement of the red emission occurs ($^4F_{9/2} \rightarrow {}^4I_{15/2}$) when pumping at 815 nm. It was proposed that two-phonon-assisted energy transfer mechanisms are mainly involved in the upconversion process with one mechanism responsible for pumping only the $^4F_{9/2}$ level, thus enhancing the red emission. Blue upconversion of the intraconfigurational $^2P_{3/2} \rightarrow {}^4I_{11/2}$ transition occurs via a three-photon ESA process.

The natural extension of this study is the investigation of the time evolution of the upconversion emission after pulsed excitation. A detailed study on the nature of the energy transfer and excited state absorption processes, using pulsed laser excitation, is in progress and will clearly explicate this point.

Acknowledgment. The authors gratefully thank Erica Viviani (Università di Verona) for expert technical assistance. The authors acknowledge the Natural Science and Engineering Research Council of Canada and MURST (Project 9903222581_005) of Italy for financial support. A. S. and M. B. affectionately remember the late Prof. G. Tessari (Università di Verona), who initiated the research on this subject.

References and Notes

(1) In Shalaev, V. M., Moskovits, M., Eds.; ACS Symposium Series 679; American Chemical Society: Washington, DC, 1998.

(2) Hong, K. S.; Meltzer, R. S.; Bihari, B.; Williams, D. K.; Tissue, B. M. *J. Lumin.* **1998**, *76* and *77*, 234−237.

(3) Soo, Y. L.; Huang, S. W.; Ming, Z. H.; Kao, Y. H.; Smith, G. C.; Goldburt, E.; Hodel, R.; Kulkarni, B.; Veliadis, J. V. D.; Bhargava, R. N. *J. Appl. Phys.* **1998**, *83*, 5404−5409.

(4) Tissue, B. M. *Chem. Mater.* **1998**, *10*, 2837−2845.

(5) Williams, D. K.; Bihari, B.; Tissue, B. M.; McHale, J. M. *J. Phys. Chem. B* **1998**, *102*, 916−920.

(6) Eilers, H.; Tissue, B. M. *Chem. Phys. Lett.* **1996**, *251*, 74−78.

(7) Bhargava, R. N. *J. Lumin.* **1997**, *72*−*74*, 46−48.

(8) Bhargava, R. N.; Chhabra, V.; Kulkarni, B.; Veliadis, J. V. *Phys. Status Solidi B* **1998**, *210*, 621−629.

(9) Bhargava, R. N. *J. Cryst. Growth* **2000**, *214*−*215*, 926−930.

(10) Goldburt, E. T.; Kulkarni, B.; Bhargava, R. N.; Taylor, J.; Libera, M. *J. Lumin.* **1997**, *72*−*74*, 190−192.

(11) Williams, D. K.; Yuan, H.; Tissue, B. M. *J. Lumin.* **1999**, *83*−*84*, 297−300.

(12) Capobianco, J. A.; Prevost, G.; Proulx, P. P.; Kabro, P.; Bettinelli, M. *Opt. Mater.* **1996**, *6*, 175−184.

(13) Kapoor, R.; Friend, C. S.; Biswas, A.; Prasad, P. N. *Opt. Lett.* **2000**, *25*, 338−340.

(14) Ye, T.; Guiwen, Z.; Weiping, Z.; Shangda, X. *Mater. Res. Bull.* **1997**, *32*, 501−506.

(15) Tessari, G.; Bettinelli, M.; Speghini, A.; Ajò, D.; Pozza, G.; Depero, L. E.; Allieri, B.; Sangaletti, L. *Appl. Surf. Sci.* **1999**, *144*−*145*, 686.

(16) Capobianco, J. A.; Vetrone, F.; D'Alesio, T.; Tessari, G.; Speghini, A.; Bettinelli, M. *Phys. Chem. Chem. Phys.* **2000**, *2*, 3203−3207.

(17) Fagherazzi, G.; Polizzi, S.; Bettinelli, M.; Speghini, A. *J. Mater. Res.* **2000**, *15*, 586−589.

(18) Polizzi, S.; Fagherazzi, G.; Battagliarin, M.; Bettinelli, M.; Speghini, A. *J. Mater. Res.* **2001**, *16*, 146−154.

(19) Kisliuk, P.; Krupke, W. F.; Gruber, J. B. *J. Chem. Phys.* **1964**, *40*, 3606−3610.

(20) Chang, N. C.; Gruber, J. B.; Leavitt, R. P.; Morrison, C. A. *J. Chem. Phys.* **1982**, *76*, 3877.

(21) Wyckoff, R. W. G. *Crystal Structures*; 2nd ed.; Interscience: New York, 1964; Vol. 2.

(22) Xu, Y.-N.; Gu, Z.-q.; Ching, W. Y. *Phys. Rev. B* **1997**, *56*, 14993−15000.

(23) Mandel, M. *Appl. Phys. Lett.* **1963**, *2*, 197.

(24) Concas, G.; Muntoni, C.; Spano, G.; Bettinelli, M.; Speghini, A. *Z. Naturforsch. A* **2001**, *56*, 267−272.

(25) Layne, C. B.; Lowdermilk, W. H.; Weber, M. J. *Phys. Rev. B* **1977**, *16*, 10−20.

(26) Riseberg, L. A.; Moos, H. W. *Phys. Rev.* **1968**, *174*, 429−438.

(27) Chamarro, M. A.; Cases, R. *J. Lumin.* **1990**, *46*, 59.

(28) Pollnau, M.; Gamelin, D. R.; Lüthi, S. R.; Güdel, H. U.; Hehlen, M. P. *Phys. Rev. B* **2000**, *61*, 3337−3346.

(29) Joubert, M. F. *Opt. Mater.* **1999**, *11*, 181−203.

(30) Zhang, H. X.; Kam, C. H.; Zhou, Y.; Han, X. Q.; Buddhudu, S.; Lam, Y. L. *Opt. Mater.* **2000**, *15*, 47−50.

(31) Chen, X.; Nguyen, T.; Luu, Q.; Bartolo, B. D. *J. Lumin.* **2000**, *85*, 295−299.